Journal of Power Sources 268 (2014) 7–13

Contents lists available at ScienceDirect

Journal of Power Sources

journal homepage: www.elsevier.com/locate/jpowsour

Al–Ga coating mechanism and discharge–charge characteristics of Li–Mn–O cathode powders at −30–55 °C

Fei-Yi Hung*, Kai-Yuan Yang

Department of Materials Science and Engineering, National Cheng Kung University, Tainan 701, Taiwan

HIGHLIGHTS

- Study of low temperature of Li battery is very importance for potential market applications.
- Al–Ga coating improved performance of the high-temperature and high C-rate charge–discharge.
- $LiMn_{2-x-y}Al_xGa_yO4$ reduces the sensitivity of the temperature effect.

ARTICLE INFO

Article history:
Received 25 January 2014
Received in revised form
3 June 2014
Accepted 4 June 2014
Available online 12 June 2014

Keywords:
Li-ion batteries
$LiMn_2O_4$
Al/Ga
Charge–discharge

ABSTRACT

In the present study, $LiMn_2O_4$ cathode powders were coated with aluminum and gallium using a solution method with two-stage surface modification to obtain a Mn-based powder with an Al–Ga surface modification layer (MAG). It was found that the MAG powders have a higher capacity and excellent cycle characteristics at 55 °C at various current rates, and that the Al–Ga coating layer inhibits the precipitation of Mn ions, which increases the stability of the structure. In addition, although low temperatures generally lead to a reduction of conductivity and capacitance, the Al–Ga coating layer gives the MAG powders low-temperature resistance, with charge–discharge characteristics better at −30 °C. The Al–Ga surface modification coating layer of $LiMn_2O_4$ powder is the $LiMn_{2-x-y}Al_xGa_yO_4$ phase, which reduces the negative impact of temperature variation. As a result, the MAG powders can be used for high C-rate charging–discharging.

1. Introduction

$LiMn_2O_4$ cathode powder is safe, inexpensive, tolerant of high working voltages, and process-stable [1–3]. It is widely accepted that $LiMn_2O_4$ cathode powder improves capacitance and cycle life by controlling the lattice structure; however, its high processing cost has limited its potential market applications [1–2]. $LiMn_2O_4$ powder at high temperatures (55 °C) and high current rate (C-rate) charge–discharge processes suffers from structural disintegration and capacity decay [3–5]. Previous studies on this material have mostly focused on doping or surface treatments to improve the charge–discharge cycle characteristics, but these processes have done little to improve high-temperature and high C-rate charge–discharge performance [6,7]. Various surface modification coating methods have been applied, such as the hydrothermal method, spray drying, the sol–gel method, and spray pyrolysis [8–11]. The solution method has been found to be simple and stable. Recently, Kang showed [12] that TiO_2-coated $LiMn_2O_4$ cathode powders prepared using in situ spray pyrolysis have high charge–discharge capacities and good cycling properties at room temperature. Therefore, cathode powders coatings can improve electrochemical properties. Furthermore, aluminum coatings can effectively enhance performance during high-temperature cycling [13]. Furthermore, adding gallium helps increase capacity [14]. In the present study, lithium manganese oxide powder (manganese-based powder, Mn based) is synthesized via a solution method that uses a two-stage coating of Al and Ga on the surface of the powders to obtain an MAG powder (Mn-based Al–Ga). The coating mechanisms and charge–discharge characteristics at high C-rates of the MAG powder are investigated.

In addition to high-temperature applications, this research can improve the low-temperature characteristics of lithium batteries [15–16]. Few studies have examined the effect of temperature on electrodes. This study analyzes the temperature effect (from 55°

* Corresponding author. Tel.: +886 6 2757575x31395; fax: +886 6 2745885.
E-mail address: fyhung@mail.ncku.edu.tw (F.-Y. Hung).

http://dx.doi.org/10.1016/j.jpowsour.2014.06.023
0378-7753/

to −30 °C) on the charge and discharge cycles of MAG electrodes. The effect of temperature on the electrochemical properties of the Al–Ga surface coating layer is discussed.

2. Experimental procedure

2.1. Powder preparation

$LiMn_2O_4$ cathode powders were synthesized following solid-state reactions used in previous studies [17]. The solution method was then used to apply an aluminum coating (first stage) followed by a gallium coating (second stage) on the surface of the lithium manganese oxide powder to obtain a cathode powder with an aluminum–gallium surface modified layer (MAG). The characteristics of the MAG powder were analyzed using scanning electron microscopy (SEM), X-ray diffraction (XRD), X-ray photoelectron spectroscopy (XPS), transmission electron microscopy (TEM), and Auger electron spectroscopy (AES). The resistance and performance of the electrode were measured in terms of cycle performance and charge–discharge curves of various C-rates. The electrochemical effects (precipitation of manganese ions, electrochemical impedance analysis, ionic conductivity of the electrolyte, temperature) were also investigated.

For the aluminum coating, citric acid mixed with $Al(NO_3)_3$ was used as a precursor. For the gallium coating, the aluminum lithium manganese oxide (MA) powder and citric acid mixed with $Ga(NO_3)_3$ were used as precursors. In both coating stages, the powders were stirred at 400 rpm at 80 °C for 100 min. The powder was then dried at 300 °C for 3 h, and then calcined at 870 °C for 12 h in air. The MAG powders were obtained after subsequent grinding and sifting. The surface of the MAG powder had an Al content of 0.33–0.81 at.% and a Ga content of 0.86–6.95 at.%.

2.2. Battery test

To perform the charge and discharge tests, an HA-CELL was assembled [17]. Tests were performed at low temperatures (−30 °C, −15 °C, 0 °C), room temperature (25 °C), and high temperature (55 °C). The actual capacity of the lithium manganese oxide was selected in 110 mAh g^{-1} of 1 C. The C-rate in the high temperature test was 0.2 C ~ 5 C. The charge–discharge tests at room temperature and low temperatures used a fixed rate of 0.2 C.

3. Results and discussion

3.1. Charge–discharge characteristics of aluminum-coated LiMnO powders at high temperature (55 °C)

Fig. 1a and b respectively shows the features of the lithium manganese oxide (M) powder and aluminum-coated lithium manganese oxide (MA) powder obtained using the solid-state reaction. The particle size of both powders is approximately 0.4–32 μm. The energy-dispersive spectroscopy (EDS) analysis results of M and MA are shown in Table 1. The Al content of MA powder in the LiMnO structure is 1.04 at.%. XRD patterns are shown in Fig. 2, which indicate that M and MA are $LiMn_2O_4$ with a cubic spinel structure [17].

Fig. 3a and b respectively shows the charge and discharge curves for various C-rates at 55 °C. At higher C-rates, the reaction time of lithium ions decreases, decreasing capacitance. Notably, the discharge capacity of M is 71 mAh g^{-1} and that of MA is 82 mAh g^{-1} (15.5% higher) for a C-rate of 5 C. The main reason is that the Al^{3+} coating shortens the distance between Mn^{3+} and Mn^{4+}, and reduces the lattice parameter and increases the conductivity of LiMnO [17,18].

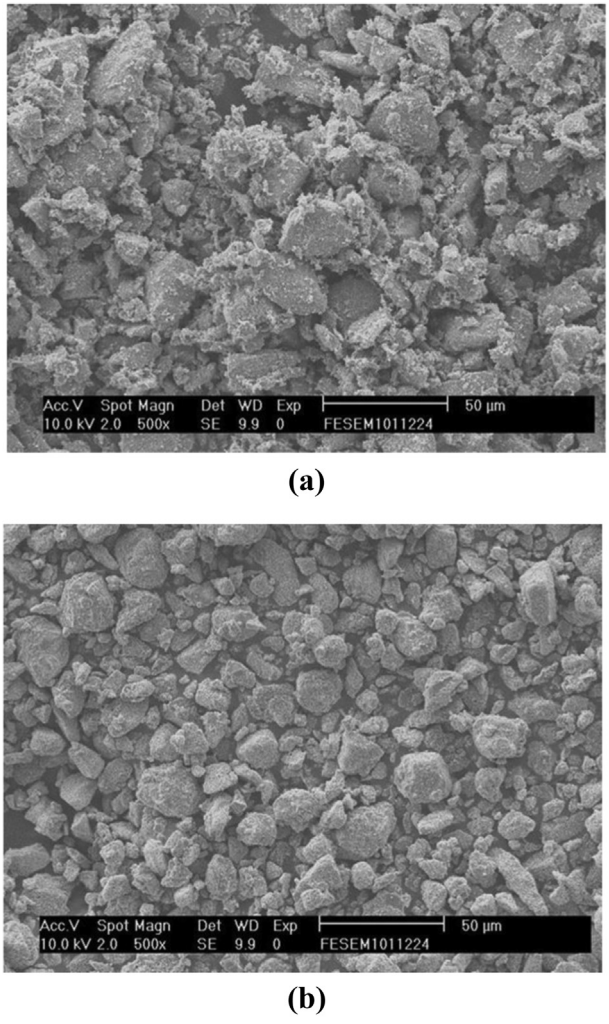

Fig. 1. Surface features of powders: (a) LiMnO (M), (b) Al coating LiMnO (MA).

Table 1
Chemical composition and symbol of Al-coating Li–Mn–O powders.

Symbol	Al (at.%)	Mn (at.%)	O (at.%)
M	0	60.22	39.78
MA	1.04	62.71	36.25

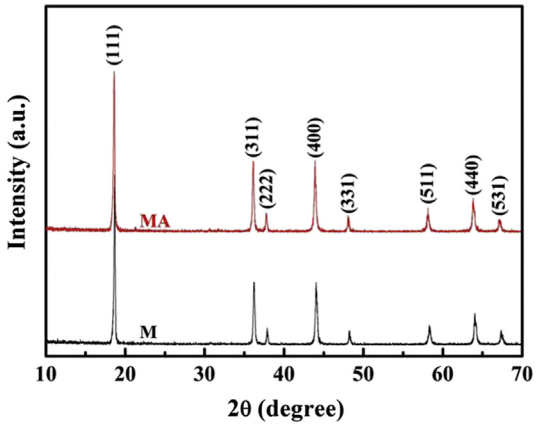

Fig. 2. XRD of LiMnO (M) and Al-coating LiMnO (MA).

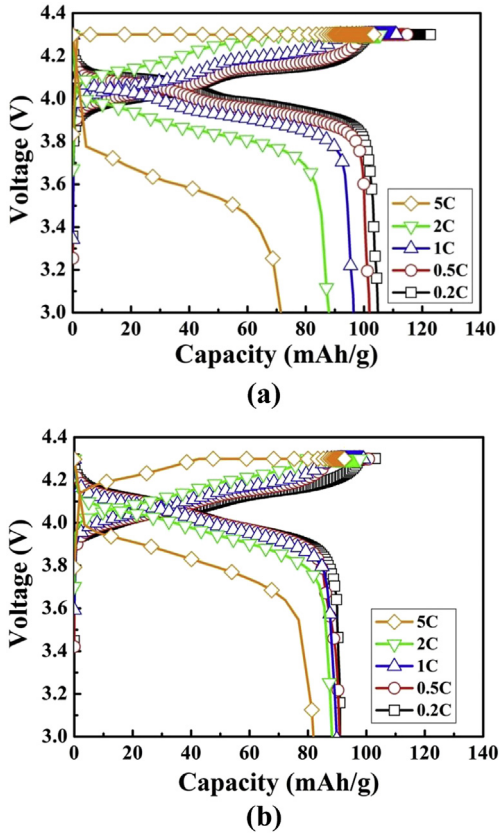

Fig. 3. The charge and discharge curves at different C-rates at 55 °C: (a) M, (b) MA.

3.2. Characteristics of Al–Ga-coated LiMnO powder

Fig. 4a and b respectively shows the surface morphologies of MAG powder and high-Ga content (MAHG) powder. The particle size of both powders is approximately 0.4–32 μm. EDS analysis results of MAG and MAHG are shown in Table 2. The Ga content levels of MAG and MAHG are 0.86 and 6.95 at.%, respectively, confirming that Ga was present in the powders. XRD patterns of the powders are shown in Fig. 5, which indicate that MA and MAG are $LiMn_2O_4$ with a cubic spinel structure. Al and Ga thus do not change the cubic spinel structure. However, the MAHG powder forms a new Ga_2O_3 phase, which has a negative effect on the material's electrochemical properties.

3.3. Bonding properties and phase analysis of MA and MAG powders

Surface coating modification affects the oxidation state of the manganese ions and the bonding energy on the surface. XPS was used for elemental energy spectrum analysis. Fig. 6a shows the Mn 2p spectra of M, MA, and MAG powders. Some small changes in the three spectra of manganese can be seen. According to the literature [18,19], the Mn $2p_{3/2}$ spectrum is characterized by Mn^{2+} (640.3 eV), Mn^{3+} (641.8 eV), and Mn^{4+} (642.8 eV) peaks. From the curve fittings of the three peaks, the integral intensity areas can be analyzed to determine the concentrations of Mn^{2+}, Mn^{3+}, and Mn^{4+}, and thus the percentage of the oxidation states.

Fig. 6b shows the Mn $2p_{3/2}$ spectra of M, MA, and MAG powders. Compared to M, the Mn^{2+} concentration for MA decreased from 11.9% to 5.2%, the Mn^{3+} concentration decreased from 44.8% to

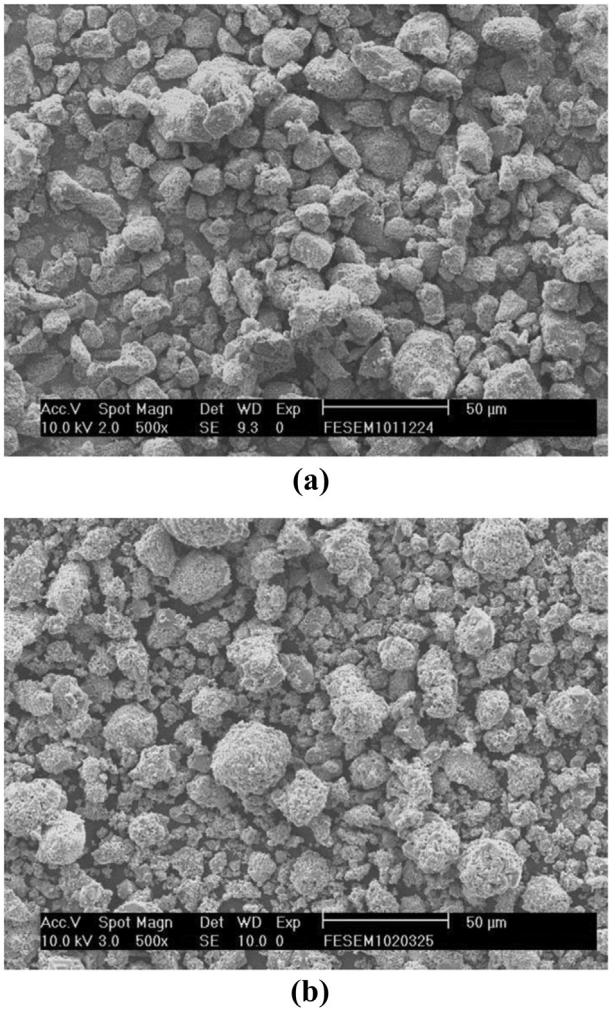

Fig. 4. Surface features of powders: (a) Ga coating LiMnO (MAG), (b) High Ga coating LiMnO (MAHG).

Table 2
Chemical composition and symbol of Al–Ga coating Li–Mn–O powders.

Symbol	Al (at.%)	Ga (at.%)	Mn (at.%)	O (at.%)
MAG	0.81	0.86	63.16	35.18
MAHG	0.33	6.95	62.26	30.46

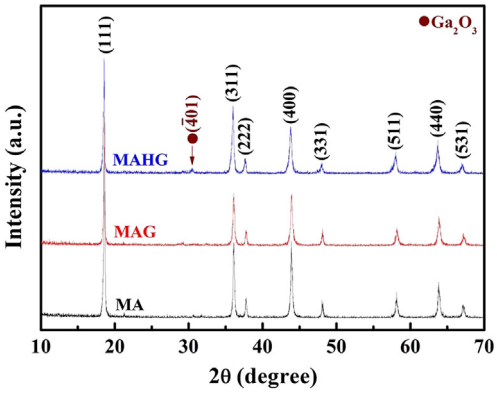

Fig. 5. XRD of Al-coating LiMnO (MA), Ga coating LiMnO (MAG) and high Ga coating LiMnO (MAHG) powders.

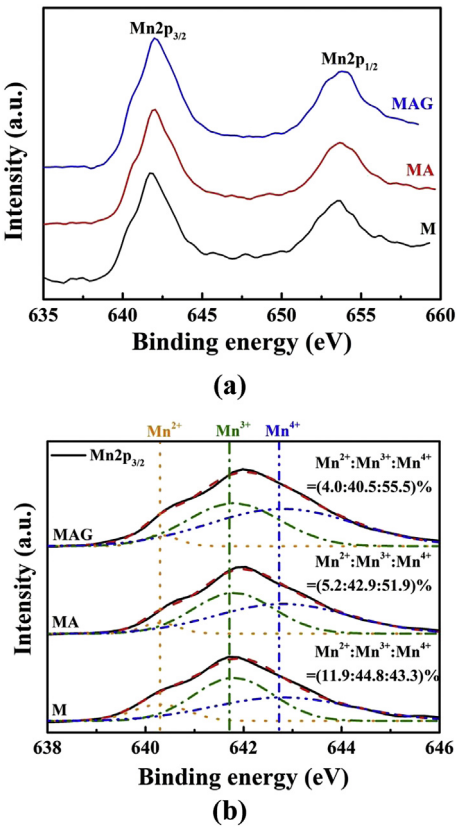

Fig. 6. X-ray photoelectron spectroscopy (XPS) of powders: (a) manganese (Mn2p), (b) manganese ($Mn2p_{3/2}$).

42.9%, and the Mn^{4+} concentration increased from 43.3% to 51.9%. The main reason for these changes is that Al^{3+} replaces Mn^{3+} on the surface of the M powder after Al coating, decreasing the Mn^{3+} concentration and increasing the Mn^{4+} concentration. This improves the manganese oxidation state of the MA powder. Further, compared to MA, the Mn^{2+} concentration for MAG decreased from 5.2% to 4.0%, the Mn^{3+} concentration decreased from 42.9% to 40.5%, and the Mn^{4+} concentration increased from 51.9% to 55.5%. The reason for these changes is that Ga^{3+} replaces Mn^{3+} on the surface of the powders, decreasing the Mn^{3+} concentration and increasing the Mn^{4+} concentration after Ga coating. This makes the oxidation state of manganese ions of MAG powder to be greater than that of MA powder. The valence of MAG powder is close to that of positive tetravalent ions.

For phase structure analysis, Fig. 7a shows the bright-field (BF) image of MA. In the rectangular area (Fig. 7b), the line profile distribution from A to B shows the percentage of aluminum atoms to be about 3 at.% or less, randomly distributed on the surface of the MA powder. TEM and EDS results confirm that Al coated the surface of the powders (Fig. 7c). Fig. 8a shows the bright-field image of MAG. The selected-area electron diffraction pattern shown in Fig. 8b shows (111) and (220) planes of the zone axes, indicating a cubic spinel structure of $Fd\bar{3}m$ (consistent with XRD analysis). Fig. 8c shows the range of line-scans from A to B, indicating that the aluminum and gallium atomic percentages are about 1–3 at.%, and are randomly distributed on the surface of the powders (Fig. 8d). Inductively coupled plasma (ICP) results of MA and MAG are shown in Table 3. The average content levels of Al and Ga are 1.06–1.31 at.%.

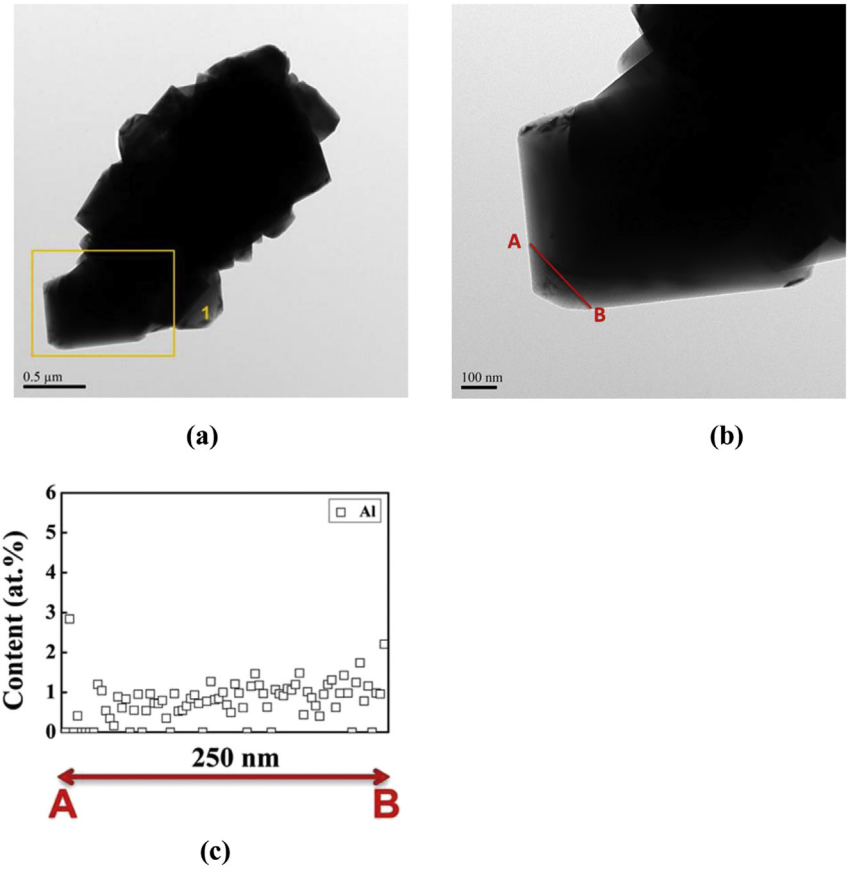

Fig. 7. Transmission electron micrograph (TEM) of MA powders: (a) bright field (BF), (b)(c) line-scan of Al in a rectangular area.

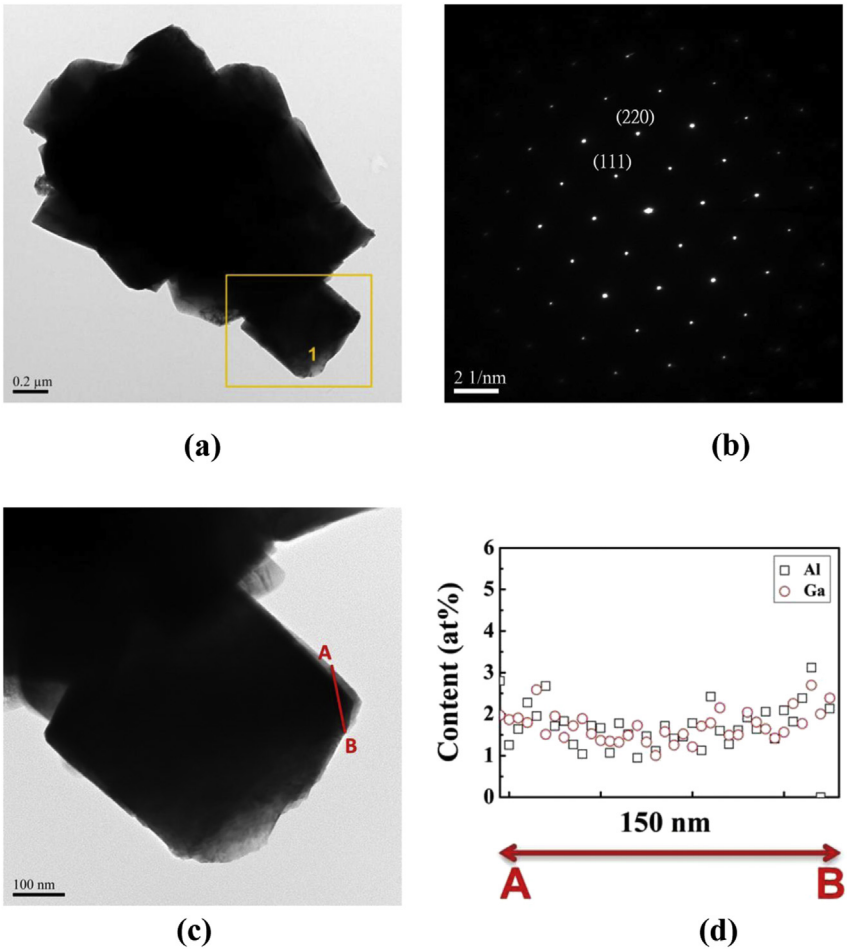

Fig. 8. Transmission electron micrograph (TEM) of MAG powders: (a) bright field (BF), (b) selected area electron diffraction pattern (SAED), (c)(d) line-scan of Al in a rectangular area.

3.4. Charge–discharge cycle characteristics of MAG powders at various C-rates and temperatures

Fig. 9a shows the first charge–discharge curve (55 °C). It can be seen that the MAG powder has a high initial capacity (111 mAh g^{-1}). Based on previous studies [12,20] and relevant circuit theory [21], the charge–discharge curves of MAG indicate a small voltage change. For a given C-rate, the internal resistance of the MAG-based battery is less than that of the MA-based battery, indicating that Ga^{3+} substitution of Mn^{3+} increases the electrode conductivity, eases Li ion migration, and improves capacity. The MAHG-based battery has a lower initial capacity (58 mAh g^{-1}), and its internal resistance is higher than that of the MAG-based battery. This result decreases the conductivity of the electrode and reduces its capacitance. The main reason is that the MAHG sample contains some Ga_2O_3 in a non-active phase, so it does not contribute to Li ion migration. Fig. 9b and c shows the coulombic efficiency and retention, respectively. The MAG and MA powders have similar coulombic efficiency and retention values. Notably, the Ga_2O_3 phase of MAHG leads to lower coulombic efficiency and retention. A compared of the relevant literature [12] and MAG, the MAG powders have better charge–discharge capacities for high C-rates. The Al–Ga coatings thus improved the electrochemical properties of the $LiMn_2O_4$ cathode powders.

Table 3
ICP of MA and MAG powders.

Symbol	Al (at.%)	Ga (at.%)
MA	0.89–1.72 (ave:1.28)	–
MAG	0.72–1.41 (ave:1.06)	0.90–1.53 (ave:1.31)

The ICP data (Table 4) show that M and MAG powders had the highest and lowest, respectively, precipitation content levels of manganese ions at high temperature (55 °C). The Al–Ga layer effectively reduces the corrosion of lithium manganese oxide caused by electrolytes.

A comparison of Figs. 3 and 10 indicates that MAG has the highest discharge capacity at 5 C (MAG: 91 mAh g^{-1}, MA: 82 mAh g^{-1}, M: 71 mAh g^{-1}). The capacity of MAG was increased due to its smaller lattice constant, Ga^{3+} doping, and the shortened distance between Mn^{3+} and Mn^{4+}.

In the low-temperature test, a four-point probe and a conductivity meter were used to measure the resistance of electrolytes and ion conductivity. Fig. 11a and b respectively shows the initial discharge capacity and the ionic conductivity of the electrolytes at various temperatures. The figures confirm that the ionic conductivity of the electrolytes is proportional to temperature; a lower temperature decreases the migration of Li ions and thus degrades capacity. Notably, the capacity of MAG was 84 mAh g^{-1} at −15 °C. Fig. 11c shows that the MAG electrodes had higher conductivity at low temperatures. This is due to the Al–Ga layer mitigating the decrease of its low-temperature capacity.

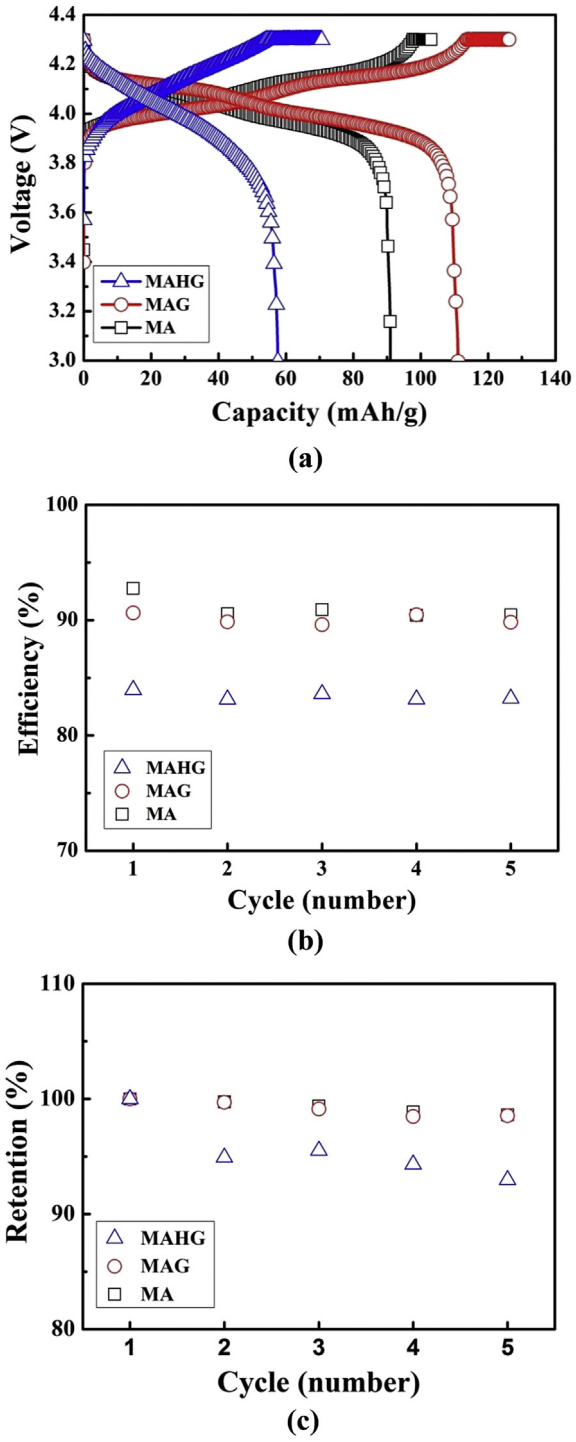

Fig. 9. The high temperature test (55 °C) of powders: (a) the first charge–discharge curve, (b) coulombic efficiency, (c) retention.

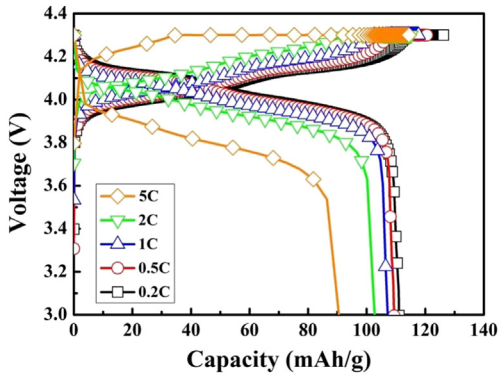

Fig. 10. The charge–discharge curves of different C-rates at 55 °C for MAG specimens.

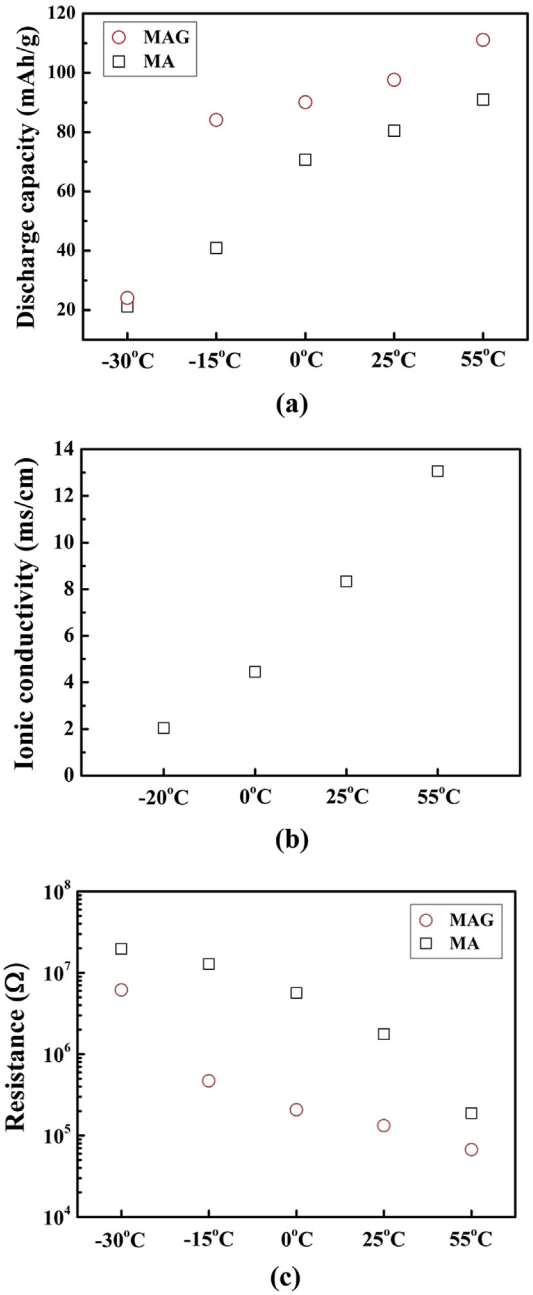

Fig. 11. Effect of temperatures for MA and MAG: (a) the initial discharge capacity in 0.2 C, (b) the ionic conductivity of electrolyte, (c) the resistance of powers.

Table 4
The precipitation content of manganese ions of all specimens in electrolyte at high temperature 55 °C.

Sample	M	MA	MAG
Mn (ppm)	20.74	16.96	9.85

Table 5
Free energy of compounds for the Al–Ga modification layer at 800 K [22–24].

Compounds	ΔG (kJ mol^{-1})
Al_2O_3	−417
Ga_2O_3	−281
Li_2O	−87
MnO	−107
MnO (Al_2O_3)	−533
$LiMn_2O_4$	−1576

3.5. Formation mechanism of Al–Ga surface modification coating layer

The free energy of related compounds at the coating surface of the Al–Ga modification layer at 800 K is shown in Table 5 [22–24]. MnO has a higher activity level than that of Al_2O_3 [23]. During the Al coating process, MnO reacts first with Al_2O_3 and then with Li_2O to form an aluminum surface layer ($LiMn_{2-x}Al_xO_4$) on the MA powder. The schematic of the coating process is shown in Fig. 12a.

During the Ga coating process, $LiMn_{2-x}Al_xO_4$ has the lowest activity level. Ga_2O_3 reacts first with MnO and then with Li_2O, forming a modified layer of gallium ($LiMn_{2-y}Ga_yO_4$). In this 2-stage of Al–Ga coatings, the MnO on the surface reacts with Al and Ga to form a modified surface layer (MnAlGaO) during the coating process. The coatings decrease the concentration of Mn^{2+}. Al^{3+} and Ga^{3+} only change the concentrations of Mn^{3+} and Mn^{4+}; therefore, the 2-stage coating forms a modified $LiMn_{2-x-y}Al_xGa_yO_4$ coating layer. The schematic of the coating process is shown in Fig. 12b. This surface coating layer improves the high-temperature charge–discharge performance and low-temperature characteristics.

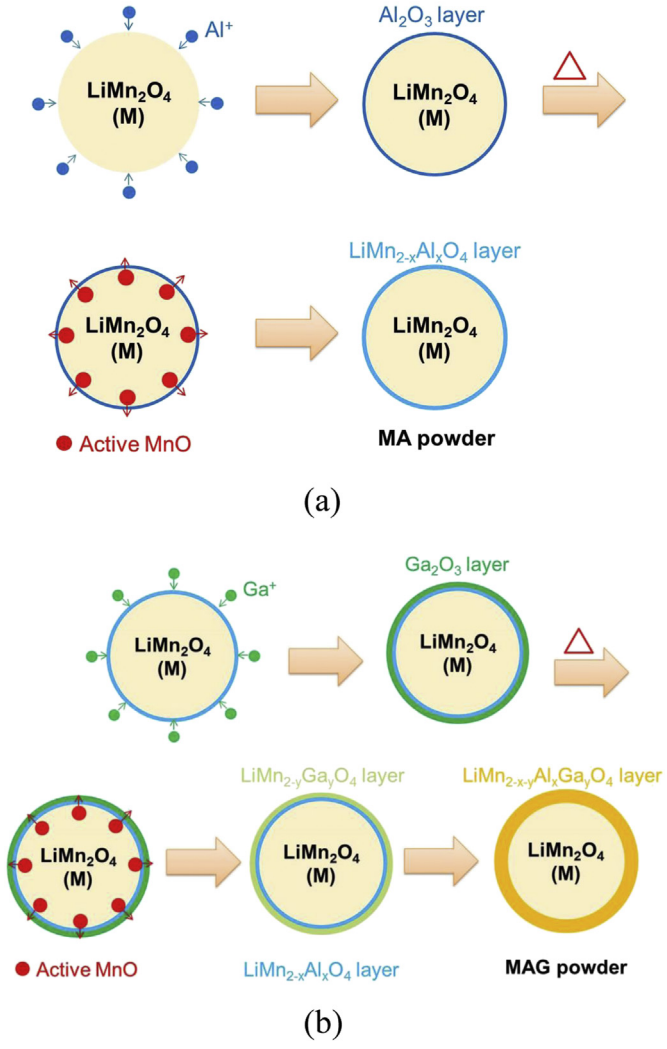

Fig. 12. Formation mechanism of surface modification coating layer: (a) MA (b) MAG.

4. Conclusion

$LiMn_2O_4$ cathode powders were coated with aluminum and gallium using a solution method with two-stage surface modification. The cations (Al^{3+}, Ga^{3+}) replaced Mn^{3+} in the MAG powder, decreasing the lattice constant, resulting in a shorter distance between Mn^{3+} and Mn^{4+} and thus improving the electronic conductivity and increasing high-C-rate performance. The $LiMn_{2-x-y}Al_xGa_yO_4$ coating layer inside Mn^{3+} does not directly contact the electrolyte, reducing the precipitation of Mn^{2+} and thus enhancing the high-temperature charge–discharge cycle stability. A low temperature, the electrolyte ionic conductivity and electrode conductivity decrease. The $LiMn_{2-x-y}Al_xGa_yO_4$ coating layer improves the low-temperature characteristics of LiMnO powder electrodes.

Acknowledgments

The authors are grateful to The Instrument Center of National Cheng Kung University for their financial support of this research under grant NSC 102-2221-E-006-061.

References

[1] Y. He, R. Li, X. Ding, L. Jiang, M. Wei, J. Alloys Compd. 492 (2010) 601–604.
[2] M. Wu, Q. Zhang, H. Lu, A. Chen, Solid State Ionics 169 (2004) 47–50.
[3] W.K. Pang, J.Y. Lee, Y.S. Wei, S.H. Wu, Mater. Chem. Phys. 139 (2013) 241–246.
[4] J. Molenda, M. Ziemnicki, J. Marzec, W. Zaj, M. Molenda, M. Bu'ckoa, J. Power Sources 173 (2007) 707–711.
[5] X. Shi, D. Zhou, Z. Zhang, L. Yu, H. Xu, B. Chen, X. Yang, Hydrometallurgy 110 (2011) 99–106.
[6] Z.P. Guo, S. Zhong, G.X. Wang, H.K. Liu, S.X. Dou, J. Alloys Compd. 348 (2003) 231–235.
[7] C. Li, H.P. Zhang, L.J. Fu, H. Liu, Y.P. Wu, E. Rahm, R. Holze, H.Q. Wu, Electrochim. Acta 51 (2006) 3872–3883.
[8] J. Xie, X. Huang, Z. Zhu, J. Dai, Ceram. Int. 37 (2011) 419–421.
[9] Z.D. Peng, Q.L. Jiang, K. Du, W.G. Wang, G.R. Hu, Y.X. Liu, J. Alloys Compd. 493 (2010) 640–644.
[10] Z.P. Guo, K. Konstantinov, G.X. Wang, H.K. Liu, S.X. Dou, J. Power Sources 119–121 (2003) 221–225.
[11] S.H. Choi, J.H. Kim, Y.N. Ko, K.M. Yang, Y.C. Kang, J. Power Sources 244 (2013) 129–135.
[12] Y.J. Hong, M.Y. Son, J.K. Lee, H.B. Lee, S.H. Lee, Y.C. Kang, J. Power Sources 244 (2013) 625–630.
[13] Z.F. Huang, C.Z. Wang, X. Meng, D.P. Wang, G. Chen, J. Solid State Chem. 179 (2006) 1602–1609.
[14] D.W. Shin, A. Manthiram, Electrochem. Commun. 13 (2011) 1213–1216.
[15] S. Ma, H. Noguchi, M. Yoshio, J. Power Sources 125 (2004) 228–235.
[16] S.R. Li, Y. Qiao, Y. Sun, S.Y. Ge, Y.M. Chen, Electrochim. Acta 81 (2012) 191–196.
[17] F.Y. Hung, T.S. Lui, H.C. Liao, Appl. Surf. Sci. 253 (2007) 7443–7448.
[18] L.S. Chang, Y.C. Lin, C.Y. Su, H.C. Wu, J.P. Pan, Appl. Surf. Sci. 258 (2011) 1279–1281.
[19] S.R. Das, I.R. Fachini, S.B. Majumder, R.S. Katiyar, J. Power Sources 158 (2006) 518–523.
[20] S.H. Kim, S.J. Kim, K.S. Nahm, H.T. Chung, Y.S. Lee, J. Kim, J. Alloys Compd. 449 (2008) 339–342.
[21] M.C. Biesinger, B.P. Payne, A.P. Grosvenor, L.W.M. Lau, A.R. Gerson, R.S.C. Smart, Appl. Surf. Sci. 257 (2011) 2717–2730.
[22] T. Aoshima, K. Okahara, C. Kiyohara, K. Shizuka, J. Power Sources 97–98 (2011) 377–380.
[23] G. Rog, W. Kucza, A.K. Rog, J. Chem, Thermodynamics 36 (2004) 473–476.
[24] I. Barin, O. Knacke, O. Kubaschewski, Thermochemical Properties of Inorganic Substances, Springer-Verlag, New York, 1973.